

Phase-Transition Process of Na₂SO₄(III) to Na₂SO₄(I) and Anharmonic Thermal Vibration

BY K. TANAKA,* H. NARUSE, H. MORIKAWA AND F. MARUMO

Research Laboratory of Engineering Materials, Tokyo Institute of Technology, Nagatsuta 4259, Midori, Yokohama 227, Japan

(Received 6 April 1990; accepted 6 February 1991)

Abstract

The crystal structure of Na₂SO₄(III) (space group *Cmcm*) and thermal motions of atoms were investigated at 298, 463 and 505 K. The cell parameters are $a = 5.6274$ (4), $b = 8.9664$ (11) and $c = 6.9737$ (9) Å at 298 K. The R and wR values were 0.0197 and 0.0202 for 984 reflections at 298 K, 0.0201 and 0.0199 for 640 reflections at 463 K, and 0.0293 and 0.0283 for 421 reflections at 505 K. A plausible process for the Na₂SO₄(III) to Na₂SO₄(I) phase transition at 520 K was proposed on the basis of the observed change in anharmonic potential with temperature. The SO₄ tetrahedra are rigid even at 505 K. The change in Na—O distances with temperature indicates that O(2), in the mirror plane at $x = 0$, becomes more mobile with increasing temperature than O(1) which is located at $z = \frac{1}{4}$ in the mirror plane. Thermal parameters indicate that O(1) is not expected to move drastically during the transition. Each significant anharmonic vibration parameter can be correlated to basic atomic motions, such as S—O bond stretching and rotation of O(2) atoms around the O(1)—O(1)' edges. Rotation of O(2) around the O(1)—O(1)' edge was found to be the main contributor to the phase transition, supporting the apex model proposed in our previous paper on the structure of Na₂SO₄(I).

Introduction

The orthorhombic modification of Na₂SO₄ (phase III) is metastable at room temperature and transforms to the hexagonal modification (phase I) at 520 K on heating (Saito, Kobayashi & Maruyama, 1982). The high-temperature modification, Na₂SO₄(I), is stable from 520 K to the melting point, 1156 K. The space group of phase I was determined to be *P6₃/mmc* by Eysel, Höffer, Keester & Hahn (1985). The crystal structure of the metastable phase, Na₂SO₄(III), was determined by Mehrotra (1981). The structure of Na₂SO₄(I) was difficult to solve

because of the lack of good-quality single crystals and the orientational disorder of the SO₄ tetrahedra which is supposed to exist after the phase transition. Arnold, Kurtz, Richter-Zinnius, Bethke & Heger (1981) proposed two possible orientations of the SO₄ tetrahedra, *i.e.*, 'apex' and 'edge' models, for the crystal structure of the high-temperature form of K₂SO₄. Based on the structure analysis of Na₂SO₄(I), stabilized by the addition of 1.2 mol% Y₂(SO₄)₃ at room temperature, Eysel *et al.* (1985) reported that the SO₄ group is statistically oriented and the edge-model orientation is the leading contributor. Further, they suggested that the apex model would be of greater importance with increasing temperature. The structure analysis of pure Na₂SO₄(I) at 693 K was carried out by Naruse, Tanaka, Morikawa, Marumo & Mehrotra (1987) and at 533 K by Mehrotra (1973), and it was found that the SO₄ groups mainly have the apex-model orientation, though coexistence of the edge-model orientation could not be eliminated. However, the detailed mechanism of the transition from phase III to I cannot be deduced from the static structures of these phases.

Analysis of thermal vibrations gives potentials where atoms are placed. The change of potential with temperature is expected to indicate possible shifts of the relevant atoms and consequently processes of the phase transition, which cannot always be determined due to degradation of the crystal upon transition. Therefore, an analysis of the thermal vibrations of the atoms in Na₂SO₄(III) was carried out by taking the third- and fourth-order anharmonic terms into account. The method used was that proposed by Dawson, Hurley & Maslen (1967) and generalized by Tanaka & Marumo (1983). Three temperatures up to just under the transition temperature were chosen in order to elucidate possible movements of the SO₄ tetrahedra upon phase transition.

Experimental

Single crystals of Na₂SO₄(III) were grown by the method described previously (Naruse *et al.*, 1987).

* Present address: Chemistry Department, Nagoya Institute of Technology, Gokiso, Showa-ku, Nagoya 466, Japan.

Table 1. *Crystal data*

Space group	<i>Cmcm</i>		
Z	4		
Temperature (K)	298	463	505
a (Å)	5.6274 (4)	5.6347 (7)	5.6330 (6)
b (Å)	8.9664 (11)	9.0344 (13)	9.0538 (10)
c (Å)	6.9737 (9)	7.0203 (7)	7.0316 (7)
V (Å ³)	351.87 (10)	357.38 (8)	358.61 (7)
D, (g cm ⁻³)	2.681	2.640	2.631
Radiation	Mo Kα	Mo Kα	Ag Kα
λ(Å)	0.71073	0.71073	0.56073
μ (cm ⁻¹)	10.15	9.99	5.20

Table 2. *Experimental conditions*

Temperature (K)	298	463	505
Radiation	Mo Kα	Mo Kα	Ag Kα
Crystal size (mm)	0.04 × 0.07 × 0.41	0.04 × 0.07 × 0.41	0.04 × 0.16 × 0.40
(sinθ/λ) _{max} (Å ⁻¹)	1.153	0.995	0.892
Scan mode	ω 2θ	ω 2θ	ω 2θ
Scan speed (min ⁻¹ in 2θ)	2.0	2.0	4.0
Scan width (A + B tanθ)			
A (°)	1.4	1.4	1.8
B (°)	0.3	0.3	0.4
Maximum No. of scans	5	5	10
No. of observed reflections [F _o > 3σ(F _o)]	984	640	421
No. of independent reflections	904	580	392

From Weissenberg photographs the space group was confirmed to be *Cmcm*. Structure determination was carried out at three temperatures, namely 298, 463 and 505 K. Specimens were attached to the tops of silica-glass capillaries using Sauereisen cement (ZrO₂-SiO₂ cement). A Pt-PtRh13% thermocouple was also fixed to the capillary, 0.3 mm from the specimen, in order to measure the temperature. The cell parameters were calculated at each temperature, using 2θ values of 19 to 26 reflections with sinθ/λ ≈ 0.7 Å⁻¹, and are listed in Table 1 together with other crystal data. Intensity data were collected on a Rigaku automated four-circle diffractometer (AFC-5UD) equipped with a heating device. The experimental conditions are summarized in Table 2. Mo Kα radiation was used for the measurements at 298 and 463 K, and Ag Kα radiation was used for the measurement at 505 K. The reflections were measured in an octant of reciprocal space. Ranges of the indices were: -5 ≤ h ≤ 12, -6 ≤ k ≤ 20, -16 ≤ l ≤ 6 for the measurement at 298 K, -11 ≤ h ≤ 5, -17 ≤ k ≤ 6, -12 ≤ l ≤ 6 at 463 K, and -2 ≤ h ≤ 11, -18 ≤ k ≤ 4, -4 ≤ l ≤ 13 at 505 K. A stream of hot nitrogen gas (Ishizawa & Kato, 1983) was used to slowly heat the crystals to the required temperatures so as to avoid crystal damage. Observed intensity data were corrected for Lorentz-polarization effects, and absorption corrections were made using the method of Busing & Levy (1957). Reflections

Table 3. *Final atomic parameters at three temperatures*

Positions of the atoms are: Na(1) (0,0,0); Na(2) (0,y,¹/₄); S (0,y,¹/₄); O(1) (x,y,¹/₄); O(2) (0,y,z). The form of anharmonic temperature factor is: exp{-2π²[h²a*²U₁₁ + k²b*²U₂₂ + l²c*²U₃₃ + 2(hka*b*U₁₂ + hla*c*U₁₃ + klb*c*U₂₃)]}.

		298 K	463 K	505 K
Na(1)	U ₁₁	0.0193 (3)	0.0340 (6)	0.0375 (12)
	U ₂₂	0.0143 (3)	0.0286 (6)	0.0317 (12)
	U ₃₃	0.0134 (3)	0.0240 (5)	0.0291 (11)
	U ₂₃	0.0013 (2)	0.0034 (5)	0.0045 (10)
Na(2)	x	0.6893 (1)	0.6891 (2)	0.6890 (3)
	U ₁₁	0.0365 (6)	0.0545 (11)	0.0581 (19)
	U ₂₂	0.0161 (3)	0.0286 (7)	0.0315 (14)
	U ₃₃	0.0222 (4)	0.0454 (9)	0.0540 (18)
S	y	0.34926 (4)	0.34877 (7)	0.34840 (14)
	U ₁₁	0.0082 (1)	0.0147 (2)	0.0157 (4)
	U ₂₂	0.0088 (1)	0.0160 (2)	0.0174 (4)
	U ₃₃	0.0097 (1)	0.0195 (2)	0.0222 (5)
O(1)	x	0.2142 (2)	0.2136 (4)	0.2135 (7)
	y	0.4455 (1)	0.4433 (2)	0.4431 (4)
	U ₁₁	0.0145 (4)	0.0254 (9)	0.0264 (18)
	U ₂₂	0.0206 (5)	0.0357 (10)	0.0392 (20)
	U ₃₃	0.0191 (5)	0.0348 (10)	0.0404 (16)
	U ₁₂	0.0085 (4)	0.0143 (9)	0.0146 (16)
O(2)	y	0.2546 (2)	0.2548 (3)	0.2556 (5)
	z	0.0787 (2)	0.0811 (4)	0.0819 (6)
	U ₁₁	0.0277 (6)	0.0511 (15)	0.0545 (27)
	U ₂₂	0.0189 (5)	0.0389 (12)	0.0436 (22)
	U ₃₃	0.0188 (5)	0.0392 (12)	0.0457 (26)
	U ₂₃	0.0097 (4)	0.0226 (10)	0.0231 (20)
	R (harmonic)	0.0203	0.0219	0.0317
	wR (harmonic)	0.0209	0.0220	0.0305
R (anharmonic)	0.0197	0.0201	0.0293	
wR (anharmonic)	0.0202	0.0199	0.0283	

with F_o > 3σ(F_o) were used in the subsequent refinements.

Refinement

Refinement with harmonic temperature factors

Atomic parameters obtained by Mehrotra (1981) were used as the starting set for the refinements. Two refinements were carried out using neutral atomic scattering factors together with those for a hypothetical partially ionic state of the constituents (Na⁺, S, O^{1/2}). Scattering factors for O^{1/2} were obtained by combining the atomic scattering factors of O (75%) and O²⁻ (25%). All atomic scattering factors except those for O²⁻ and anomalous-dispersion terms were taken from *International Tables for X-ray Crystallography* (1974, Vol. IV). The scattering factors given by Tokonami (1965) were used for O²⁻.

The refinement using atomic scattering factors for the partially ionic model resulted in better R values. For example, R = ∑|F_o - F_c| / ∑|F_o| and wR = [∑(|F_o - F_c|)² / ∑F_o²]^{1/2} for the data at 298 K were 0.0214 and 0.0224 respectively for the neutral-atom

Table 4. Unit vectors along principal axes of thermal ellipsoids based on the lattice system; $\mathbf{u} = x\mathbf{a} + y\mathbf{b} + z\mathbf{c}$

S	298 K			463 K			505 K		
	x	y	z	x	y	z	x	y	z
$\mathbf{u}_1(\parallel \mathbf{a})$	0.178	0.0	0.0	0.178	0.0	0.0	0.178	0.0	0.0
$\mathbf{u}_2(\parallel \mathbf{b})$	0.0	0.112	0.0	0.0	0.111	0.0	0.0	0.111	0.0
$\mathbf{u}_3(\parallel \mathbf{c})$	0.0	0.0	0.143	0.0	0.0	0.142	0.0	0.0	0.142
O(1)									
\mathbf{u}_1^o	-0.146	-0.064	0.0	-0.145	-0.064	0.0	-0.149	-0.061	0.0
\mathbf{u}_2^o	-0.102	0.091	0.0	-0.107	0.091	0.0	-0.098	0.093	0.0
$\mathbf{u}_3(\parallel \mathbf{c})$	0.0	0.0	0.143	0.0	0.0	0.142	0.0	0.0	0.142
O(2)									
$\mathbf{u}_1(\parallel \mathbf{a})$	0.178	0.0	0.0	0.178	0.0	0.0	0.178	0.0	0.0
\mathbf{u}_2^o	0.0	-0.079	-0.101	0.0	-0.078	0.101	0.0	-0.080	-0.098
\mathbf{u}_3^o	0.0	0.079	0.101	0.0	0.078	0.101	0.0	-0.077	0.103

Notes: (a) The angle between \mathbf{u}_1 and S—O(1) is 0.3°. (b) Approximately perpendicular to S—O(1). (c) The angle between \mathbf{u}_2 and S—O(2) is 9.2°. (d) Approximately perpendicular to S—O(2).

model, and 0.0203 and 0.0209 for the partially ionic model. The 200 reflection is most significantly affected by extinction, and the structure-factor values at 298, 463 and 505 K were decreased by 43, 26 and 17%, respectively, as estimated from extinction correction factors based on the anisotropic type-I extinction effect assumption (Becker & Coppens, 1974*a,b*, 1975). The final atomic parameters are listed in Table 3.

Refinement with anharmonic temperature factors

In order to analyze the thermal motion of atoms near the transition temperature, refinement of the anharmonic temperature factors was carried out. If a crystal is assumed to be made up of an assembly of independent oscillators obeying Boltzmann statistics, the temperature factor for an atom with anharmonic thermal vibration is expressed (Dawson *et al.*, 1967; Willis, 1969) as,

$$\langle \exp(2\pi i \mathbf{S} \cdot \mathbf{u}) \rangle = \iiint \exp(2\pi i \mathbf{S} \cdot \mathbf{u}) \exp[-V(\mathbf{u})/kT] d\mathbf{u} / \iiint \exp[-V(\mathbf{u})/kT] d\mathbf{u}, \quad (1)$$

where k and T are Boltzmann's constant and the temperature of the system, respectively. \mathbf{S} is the scattering vector and $\langle \rangle$ indicates the mean value. The potential V of an atom in a crystal expressed, for the general case, in terms of the displacement vector \mathbf{u} from the equilibrium position is as follows (Tanaka & Marumo, 1983),

$$\begin{aligned} V(\mathbf{u}) = & V_0 + \frac{1}{2} \sum_i b_i u_i^2 + \sum_{i,j} c_{ijj} u_i u_j^2 + c_{123} u_1 u_2 u_3 \\ & + \sum_{i \geq j} q_{ijij} u_i^2 u_j^2 + \sum_{i \neq j} q_{ijij} u_i^3 u_j \\ & + \sum_i' q_{ijk} u_i^2 u_j u_k, \end{aligned} \quad (2)$$

where u_1 , u_2 and u_3 are the magnitudes of components of the displacement vector defined on the

Cartesian coordinate system as determined by the three principal axes of the thermal ellipsoid of each atom. V_0 is the potential of the atom at the equilibrium position. \sum_i' means summation over i under the condition that subscripts i, j and k are different from each other and no permutation of j and k is permitted. The unit vectors along the principal axes of the thermal ellipsoids are listed in Table 4 for the respective atoms and their orientations are illustrated in Fig. 1. The u_1 and u_2 axes of O(1) and S lie in the mirror plane at $z = \frac{1}{4}$, where O(1), O(1)' and S lie. The u_2 and u_3 axes of O(2) are in the mirror plane at $x = 0$, which contains O(2), O(2)' and S. The u_2 axis of S points towards the middle of the O(1)—O(1)' edge and the u_2 axis of O(2) also points approximately to it.

The anharmonic temperature factors were refined by fixing the atomic coordinates and harmonic temperature factors to the values obtained by the previous refinements. Since the point symmetries of the S, O(1) and O(2) atoms are $m2m(2//b)$, $m(\perp c)$ and

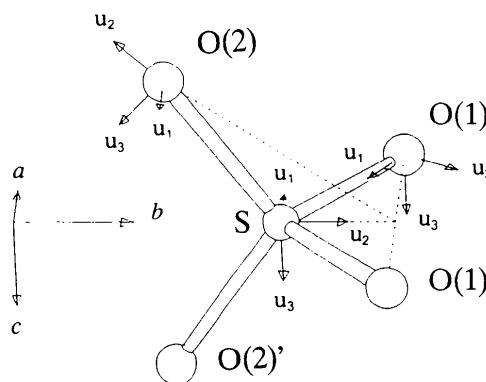


Fig. 1. The local Cartesian coordinate system in SO_4 . \mathbf{u}_1 , \mathbf{u}_2 and \mathbf{u}_3 are the unit vectors along the principal axes of the thermal ellipsoid of each atom.

Table 5. Harmonic ($\times 10^{-19}$ J Å⁻²) and anharmonic third-order ($\times 10^{-19}$ J Å⁻³) and fourth-order ($\times 10^{-19}$ J Å⁻⁴) potential parameters (e.s.d.'s in parentheses)

	298 K	463 K	505 K
S			
<i>b</i> ₁	4.99 (6)	4.35 (6)	4.45 (12)
<i>b</i> ₂	4.68 (5)	3.99 (5)	4.01 (10)
<i>b</i> ₃	4.26 (5)	3.29 (4)	3.14 (7)
<i>c</i> ₂₁₁	0.2 (10)	-1.3 (6)	-1.9 (13)*
<i>c</i> ₂₂₂	-1.2 (5)	-0.3 (2)	-0.07 (44)
<i>c</i> ₂₃₃	0.2 (8)	1.8 (4)	1.4 (8)
<i>q</i> ₁₁₁₁	-2.4 (33)	-1.2 (14)	1.9 (29)
<i>q</i> ₁₁₂₂	1.4 (139)	1.0 (55)	-21.4 (126)*
<i>q</i> ₁₁₃₃	11.0 (121)	4.3 (41)	9.5 (79)
<i>q</i> ₂₂₂₂	2.5 (28)	0.4 (11)	3.4 (23)
<i>q</i> ₂₂₃₃	15.2 (110)	-3.2 (38)	-1.2 (74)
<i>q</i> ₃₃₃₃	0.8 (23)	-0.1 (7)	-1.1 (13)
O(1)			
<i>b</i> ₁	4.83 (22)	4.15 (25)	4.13 (43)
<i>b</i> ₂	1.55 (2)	1.40 (3)	1.43 (5)
<i>b</i> ₃	2.15 (5)	1.84 (5)	1.73 (9)
<i>c</i> ₁₁₁	0.8 (6)	0.7 (5)	0.4 (9)
<i>c</i> ₁₂₂	-0.9 (4)	-0.5 (4)	-0.06 (71)
<i>c</i> ₁₃₃	-0.2 (7)	0.4 (5)	-0.6 (9)
<i>c</i> ₂₁₁	0.4 (8)	0.5 (6)	-0.09 (12)
<i>c</i> ₂₂₂	0.10 (9)	0.06 (8)	0.03 (15)
<i>c</i> ₂₃₃	-0.6 (3)	-0.6 (2)	-0.1 (4)
<i>q</i> ₁₁₁₁	4.2 (53)	-1.0 (29)	2.6 (53)
<i>q</i> ₁₁₂₂	-8.1 (67)	-1.0 (40)	1.3 (76)
<i>q</i> ₁₁₃₃	-3.2 (114)	3.3 (59)	-11.6 (102)*
<i>q</i> ₂₂₂₂	0.5 (4)	-0.07 (28)	-0.4 (5)
<i>q</i> ₂₂₃₃	0.3 (21)	-0.05 (12)	2.1 (22)
<i>q</i> ₃₃₃₃	0.2 (10)	-0.3 (5)	0.5 (8)
<i>q</i> ₁₁₁₂	4.1 (82)	1.4 (45)	-5.3 (92)
<i>q</i> ₂₂₁₂	0.1 (3)	-0.2 (15)	1.3 (31)
<i>q</i> ₃₃₁₂	-7.2 (76)	-1.4 (44)	3.4 (82)
O(2)			
<i>b</i> ₁	1.49 (3)	1.25 (4)	1.28 (6)
<i>b</i> ₂	4.53 (22)	3.89 (26)	3.24 (33)
<i>b</i> ₃	1.44 (2)	1.04 (2)	1.03 (3)
<i>c</i> ₂₁₁	0.7 (4)	1.0 (3)	1.1 (6)*
<i>c</i> ₂₂₂	-1.4 (5)	-1.8 (4)	-1.8 (6)*
<i>c</i> ₂₃₃	0.9 (4)	1.0 (3)	1.2 (4)*
<i>c</i> ₃₁₁	-0.2 (2)	-0.2 (1)	-0.4 (2)*
<i>c</i> ₃₂₂	0.9 (7)	-0.3 (5)	0.6 (7)
<i>c</i> ₃₃₃	-0.03 (9)	0.08 (5)	0.04 (8)
<i>q</i> ₁₁₁₁	-0.2 (4)	-0.1 (2)	0.4 (4)
<i>q</i> ₁₁₂₂	1.0 (59)	1.9 (33)	-3.3 (49)
<i>q</i> ₁₁₃₃	1.0 (13)	0.05 (58)	-0.8 (11)
<i>q</i> ₂₂₂₂	0.07 (37)	-0.9 (24)	1.4 (28)
<i>q</i> ₂₂₃₃	-2.6 (57)	-0.08 (273)	-0.3 (39)
<i>q</i> ₃₃₃₃	0.2 (42)	-0.004 (146)	0.1 (3)
<i>q</i> ₁₁₂₁	3.0 (42)	-0.3 (21)	-2.8 (34)
<i>q</i> ₂₂₂₁	-4.7 (69)	1.9 (33)	1.8 (5)*
<i>q</i> ₃₃₂₁	0.7 (22)	0.7 (9)	0.1 (2)

* See text.

m(\perp **a**) respectively, these atoms have three, six and six symmetry-permitted third-order anharmonic parameters, and eight, nine and nine fourth-order parameters, respectively. Refinements were carried out using the program *LINKT80* which was coded

Table 6. Bond lengths (Å) and angles (°)

	298 K	463 K	505 K	
S—O(1)	1.482 (1)	1.475 (2)	1.477 (4)	
S—O(1) ^a	1.489 (1)	1.486 (2)	1.488 (4)	
S—O(2)	1.466 (1)	1.459 (3)	1.450 (4)	
S—O(2) ^a	1.476 (2)	1.478 (3)	1.472 (4)	
O(1)—O(1)	2.411 (2)	2.405 (3)	2.393 (5)	
O(1)—O(1) ^a	2.422 (2)	2.423 (3)	2.424 (5)	
O(1)—O(2)	2.411 (2)	2.400 (3)	2.406 (5)	
O(1)—O(2) ^a	2.424 (2)	2.424 (3)	2.420 (5)	
O(2)—O(2)	2.390 (2)	2.374 (4)	2.363 (6)	
O(2)—O(2) ^a	2.406 (2)	2.404 (4)	2.398 (6)	
O(1)—S—O(1)	108.83 (8)	109.2 (1)	109.1 (2)	
O(1)—S—O(2)	109.70 (4)	109.7 (1)	109.7 (1)	
O(2)—S—O(2)	109.20 (8)	108.8 (2)	109.1 (3)	
				$\langle \Delta(\text{Na—O}) \rangle$
Na(1)—O(1)	2.4218 (9)	2.439 (2)	2.441 (3)	0.019
Na(1)—O(2)	2.347 (1)	2.373 (3)	2.384 (5)	0.037
Na(2)—O(1)	2.804 (2)	2.807 (2)	2.810 (4)	0.006
Na(2)—O(1)	2.497 (2)	2.526 (2)	2.531 (4)	0.034
Na(2)—O(2)	2.347 (1)	2.381 (3)	2.388 (4)	0.041

Notes: (a) Corrected values with the riding-motion model. (b) Calculated using the corrected S—O bond lengths with the equation, $(\text{O—O}) = 2(\text{S—O})\sin(\angle\text{O—S—O})$. (c) Calculated using the corrected S—O bond lengths with the equation, $\text{O—O} = \{(\text{S—O})^2 - 2[\text{S—O}(1)][\text{S—O}(2)]\cos[\angle\text{O}(1)—\text{S—O}(2)]\}^{1/2}$.

by one of the authors (KT). *V*(**u**) values of S, O(1) and O(2) are listed in Table 5.*

Results and discussion

Shift of atomic parameters with temperature

In order to obtain the basic framework of the transition process from phase III to I, changes in the atomic parameters with temperature were examined. Since both the cell dimensions and fractional coordinates of atoms shift with temperature, the structural changes can be understood more easily by comparing the bond lengths and angles (listed in Table 6). After correction for 'riding motion' (Busing & Levy, 1964), the S—O bond lengths coincide with each other within the experimental errors at the three temperatures. The O—S—O bond angles show a slight deviation from the tetrahedral angle of 109.47° and do not change with temperature. Accordingly it is concluded that SO₄ tetrahedra are rigid and are expected to keep their shape during the phase-transition process. O(1) has four nearest neighbour Na atoms, whereas O(2) has only two. The differences in the Na—O distances at 505 and 298 K [$\Delta(\text{Na—O})$'s in Table 6] indicate that the elongation of the Na—O(2) distances is larger than for the Na—O(1) distances,

* Lists of structure factors at 298, 463 and 505 K have been deposited with the British Library Document Supply Centre as Supplementary Publication No. SUP 53984 (27 pp.). Copies may be obtained through The Technical Editor, International Union of Crystallography, 5 Abbey Square, Chester CH1 2HU, England.

although the Na—O(2) distances are shorter than those of Na—O(1). These facts suggest that O(2) becomes mobile with temperature more rapidly than O(1).

Mean-square displacements of S, O(1) and O(2) were calculated from harmonic temperature factors and are plotted against temperature in Fig. 2. The mean-square displacements of O(2) along the two directions (u_1 and u_3) perpendicular to the S—O bond increase with temperature more rapidly than those of O(1). Increments of the mean-square displacements of O(1) and O(2) along the S—O bonds are approximately equal to each other, and the magnitudes are comparable to the three components u_1 , u_2 and u_3 of S. The curves along the u_3 axis of O(1), the u_2 axis of O(2) and the u_3 axis of S exhibit clear deviations from linear relations at higher temperatures, which indicates the existence of anharmonic character in the thermal vibrations. Non-linear features along the u_1 and u_3 axes of O(2) are not obvious since the magnitudes of mean-square displacements increase rapidly. We will need more data at lower temperatures to clarify the anharmonic character of the vibration of O(2).

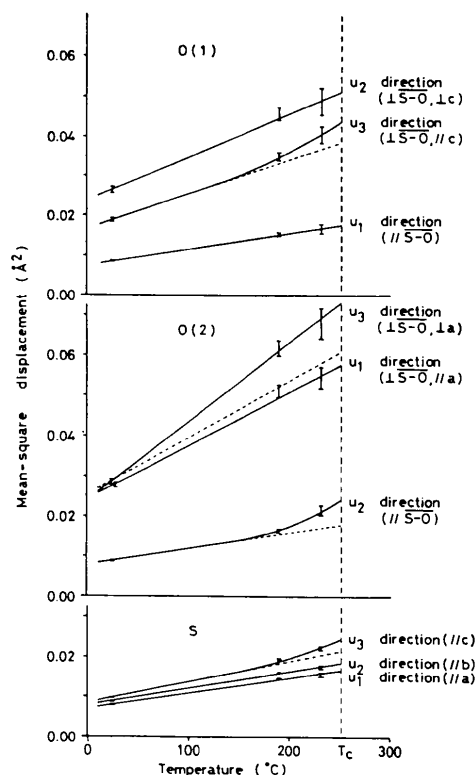


Fig. 2. Mean-square displacement of S, O(1) and O(2) along the principal axes of their thermal ellipsoids. //S—O or \perp S—O indicates that the direction of the principal axis is approximately parallel or perpendicular, respectively, to the S—O bond, except u_1 of O(2) which is exactly perpendicular to S—O.

Deformation density

In order to examine the effect of anharmonic vibrations of atoms on the charge density in Na_2SO_4 , difference density maps, $\Delta\rho_{\text{harm}}$ and $\Delta\rho_{\text{anharm}}$, were calculated after the harmonic and anharmonic refinements, respectively. Since the effect of thermal vibration is more important in higher-order reflections and outer-shell valence electrons have more influence on lower-order reflections, the two effects are expected to be at least partially separable on deformation density maps. This was shown to be the case in the charge density study on KCuF_3 (Tanaka, Konishi & Marumo, 1979; Tanaka & Marumo, 1982). The deformation density due to the anharmonic vibration is also expected to increase with temperature (Yamanaka, Takeuchi & Tokonami, 1984), and it becomes especially prominent when the temperature approaches the transition point (Sakata, Harada, Cooper & Rouse, 1980).

$\Delta\rho_{\text{harm}}$ maps at 505 K were compared with the accurate charge density determined for CaSO_4 by Kirfel & Will (1980, 1981) at room temperature. Fig. 3 shows $\Delta\rho_{\text{harm}}$ in the plane at $z = 0.25$, where S and two O(1) atoms lie. It has the following features which are quite similar to those observed by Kirfel & Will (1980) for CaSO_4 : (a) σ -bond peaks are observed on the S—O(1) bonds; (b) there is a positive peak on the line connecting O(1) and Na(2); (c) a polarization peak belonging to Na(2) exists. However, the electron cloud of Na(2) is polarized toward the O(2) atoms in contrast to the polarization of Ca^{2+} in CaSO_4 . Fig. 4 shows $\Delta\rho_{\text{harm}}$ in the plane at $x = 0$, where S and two O(2) atoms lie. The following peaks are observed in Fig. 4: (a) σ -bond peaks on S—O(2) bonds; (b) peaks on the lines connecting

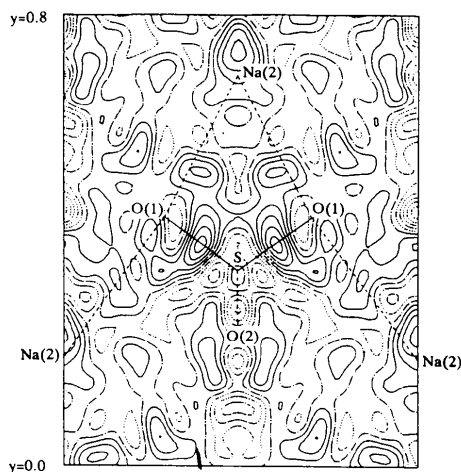


Fig. 3. Dynamic deformation density map at 505 K on the plane of S and two O(1) atoms. Contours at $0.2 \text{ e } \text{\AA}^{-3}$. Negative and zero contours are shown in broken and dashed-dotted lines, respectively.

O(2) and Na(1), and O(2) and Na(2). Kirfel & Will (1980) found a peak near the S atom on the bisectrix of the O(2)—S—O(2)' angle in CaSO_4 and attributed it to the $d\pi$ bond character of the S—O bonds. Though a similar peak can only be observed on the map at 298 K in the present study, the peaks on the S—O bonds are significantly elongated perpendicular to the bonds at all temperatures, indicating $d\pi$ character of the bonds (Cruickshank, 1961).

An increase in peak height with temperature is observed for several peaks in the deformation density maps, despite severe thermal smearing, which indicates that these peaks are due to anharmonic vibration. The peak and trough (Fig. 4) around O(2) on the O—S bond and its extension become more prominent with increasing temperature. The peak heights are 0.6, 1.0 and 1.0 $e \text{ \AA}^{-3}$, at 293, 463 and 505 K, and the depths of the troughs at these temperatures are -0.4, -0.6 and -1.0 $e \text{ \AA}^{-3}$, respectively. The trough on the left-hand side of S in Fig. 4 and the peak in the middle of the line Na(2)—O(1) in Fig. 3 also become larger at 505 K. On the other hand the polarization peak above Na(2) in Fig. 3 becomes less prominent at 505 K.

Figs. 5 and 6 show $\Delta\rho_{\text{anharmonic}}$ at 505 K. The features around Na(2) and O(1) in Fig. 5 show no significant difference from Fig. 3. However, the trough just below the S atom in Fig. 3 is significantly diminished in Fig. 5 and the σ -bond peak on the S—O(1) bond is lowered and more elongated perpendicular to the S—O(1) bond. This may indicate correlation of the anharmonic vibration effect with the bonding electrons. Fig. 6 shows that peaks around O(2) display significantly diminished heights after anharmonic vibration refinement. The trough on the bisectrix of

the O(2)—S—O(2)' angle disappears in Fig. 6. This implies that the trough on the bisectrix found in $\Delta\rho_{\text{harm}}$ at 505 K is due to the anharmonic vibration effect.

Potential parameters

Significant anharmonic potential parameters which have absolute values larger than three times their e.s.d.'s, or have values larger than their e.s.d.'s and increase with temperature, are marked with an asterisk in the 505 K column in Table 5, since the anharmonic vibration is expected to be enhanced significantly near the phase-transition temperature as

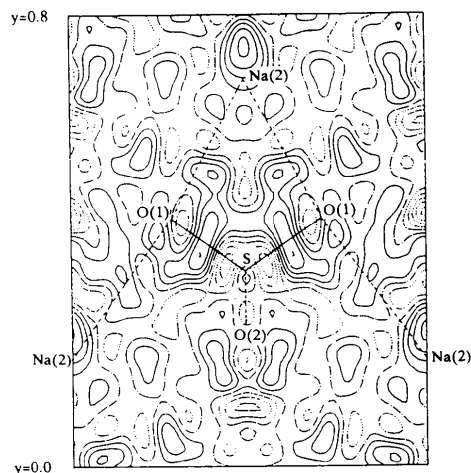


Fig. 5. Residual map at 505 K after the anharmonic vibration analysis on the same plane as Fig. 3. Contours at $0.2 e \text{ \AA}^{-3}$. Negative and zero contours are shown in broken and dashed-dotted lines, respectively.

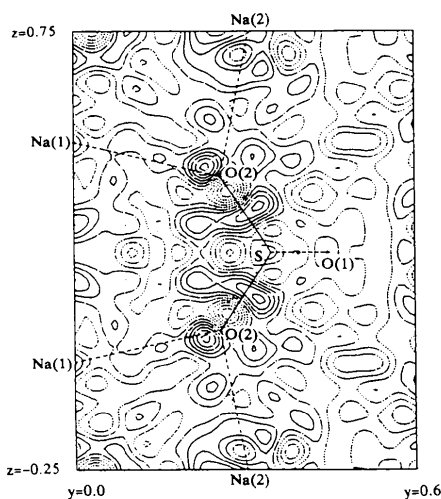


Fig. 4. Dynamic deformation density map at 505 K on the plane of S and two O(2) atoms. Contours at $0.2 e \text{ \AA}^{-3}$. Negative and zero contours are shown in broken and dashed-dotted lines, respectively.

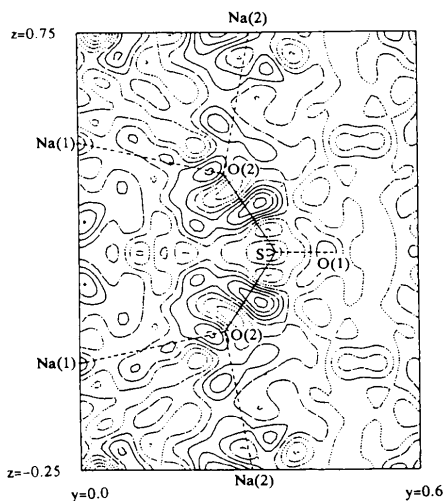


Fig. 6. Residual map at 505 K after the anharmonic vibration analysis on the same plane as Fig. 4. Contours at $0.2 e \text{ \AA}^{-3}$. Negative and zero contours are shown in broken and dashed-dotted lines, respectively.

stated in the previous section. Anharmonic thermal vibration of O(1) is indistinct in accordance with the features of the deformation density maps shown in Figs. 3 and 6. q_{1133} of O(1) is a component of the centrosymmetric potential and cannot shift the average position of O(1), though its change at 505 K is remarkable. O(2) and S have significantly large third-order anharmonic potential parameters.

The anharmonic part of the potential of O(2) in the mirror plane at $x = 0$ ($u_1 = 0$) was calculated using only the significant cubic potential parameters c_{222} and c_{233} as shown in Fig. 7. The quartic term q_{2223} was not included in the calculation, since the potential due to it was one order smaller than those due to cubic terms in the vicinity of O(2). Since only significant terms were used in the calculation, the u_2 axis becomes tentatively a non-crystallographic two-fold axis. The c_{233} value obtained gives negative potentials in the region where the coordinate u_2 is negative and $|u_3|$ is large compared with $|u_2|$ as seen in Fig. 7. The positive c_{233} value may be correlated to the rotation of O(2) around an axis parallel to [100], which is parallel to O(1)—O(1)' and running through a point on the same side of O(2) as S. In general, a positive c_{ijj} value, where i and j are different from each other, represents the potential which is correlated to rotation of the relevant atom around the axis parallel to the remaining axis u_k and passing through a point on the u_i axis on the negative side of it. It is worthy of note that the apex-model structure for $\text{Na}_2\text{SO}_4(\text{I})$ is obtained from the structure of $\text{Na}_2\text{SO}_4(\text{III})$, if the SO_4 group is rotated around the O(1)—O(1)' edge. Since c_{211} of O(2) has a similar value to c_{233} , a similar feature is observed on the u_1 — u_2 section of the potential, indicating a rotation of

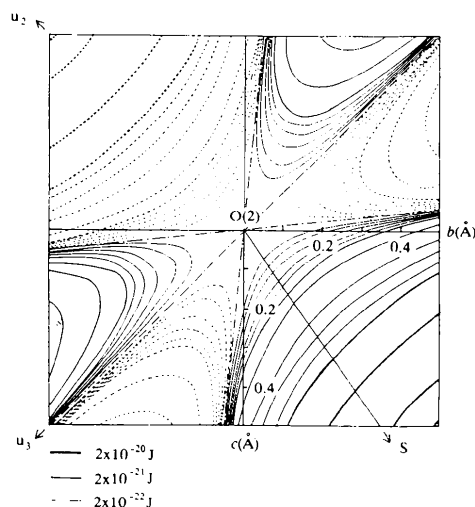


Fig. 7. Anharmonic potential of O(2) on the plane of S and two O(2) atoms. Negative and zero contours are shown in broken and dashed-dotted lines, respectively.

O(2) around an axis parallel to the u_3 axis. Rotation of the SO_4 group around this axis means the O(1) atoms move drastically, which contradicts the fact that the potential of O(1) gives no indication of such a rotation. Therefore, the possible rotation indicated by the significant c_{211} value of O(2) is not a contributor to the phase transition but to the instantaneous deformation of SO_4 . The third-order parameter c_{211} of S, which is correlated to the rotation around the c axis, is also rejected as a possible contributor to the transition for the same reason. The negative q_{1122} value of S favours movement of the atom in the xy plane.

The u_2 axis of O(2) lies approximately along the S—O(2) bond. The positive and negative potentials observed on the bond and its extension in Fig. 7 simply indicate that the bond is more difficult to compress than to expand. The feature shown in the potential diagram corresponds to the pair of positive and negative peaks around O(2) in Fig. 4, though these peaks seem to be partially due to the aspherical distribution of valence electrons of O(2), since they still remain in the $\Delta\rho_{\text{anharmonic}}$ map in Fig. 6.

Concluding remarks

In Fig. 8, arrangements of SO_4 tetrahedra in (a) apex and (b) edge models for phase I are illustrated by broken lines. In the apex model one of the apices of SO_4 is located on the threefold axis. If the apex model corresponds to the true structure of phase I, the O(2) atoms should rotate around the O(1)—O(1)' edge parallel to the a axis in order to transform from phase III to phase I, because one of the O(2) atoms as well as the S atom are located on the threefold axis in the apex model. In the edge model, one of the edges of the SO_4 tetrahedron is parallel to the c axis and one of the remaining edges lies in the mirror plane at $z = \frac{1}{4}$. Three tetrahedra are statistically superimposed in accordance with the threefold rotational symmetry of the crystal. Since there are three kinds of edges, O(1)—O(1)', O(2)—O(2)' and O(1)—O(2) in $\text{Na}_2\text{SO}_4(\text{III})$, three possible ways exist to derive the edge-model structure. Least movement

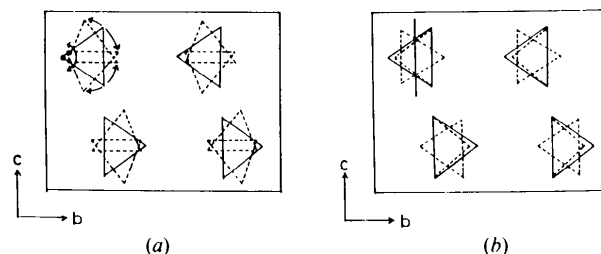


Fig. 8. Crystal structure of (a) the 'modified apex model' and (b) the 'edge model' viewed down the c axis.

is required in the process of arranging O(1)—O(2) parallel to [001]. In all of these ways all the O atoms in SO₄ must move in order to yield the 'edge-model' structure.

The SO₄ tetrahedra are supposed to be rigid during the phase-transition process and O(2) is more mobile than O(1) as discussed in the present work. The small anharmonic parameters of O(1) suggest that O(1) does not move drastically during the transition. The parameter c_{233} of O(2) is correlated to rotation around a line parallel to [100] through a point lying on the same side as S with respect to O(2). Since the u_2 axis of O(2) is almost parallel to the line between O(2) and the midpoint of O(1)—O(1)', and O(1) atoms are not expected to move drastically, the positive c_{233} value of O(2) is thought to be correlated to rotation of the SO₄ tetrahedron around the O(1)—O(1)' edge. The upward and downward rotations with respect to the z direction may occur with equal probability, since there are two negative potential regions at both sides of the O—S bond in Fig. 7, which are equivalent to each other within the present approximation. Thus, the mirror plane at $z = \frac{1}{4}$, which is required by the space group of the high-temperature form, is preserved. This phase-transition mechanism does not contradict evidence obtained in the study of the high-temperature phase and supports the structure of phase I reported in the previous paper (Naruse *et al.*, 1985).

References

- ARNOLD, H., KURTZ, W., RICHTER-ZINNIUS, A., BETHKE, J. & HEGER, G. (1981). *Acta Cryst.* **B37**, 1643–1651.
- BECKER, P. J. & COPPENS, P. (1974a). *Acta Cryst.* **A30**, 129–147.
- BECKER, P. J. & COPPENS, P. (1974b). *Acta Cryst.* **A30**, 148–153.
- BECKER, P. J. & COPPENS, P. (1975). *Acta Cryst.* **A31**, 417–425.
- BUSING, W. R. & LEVY, H. A. (1957). *Acta Cryst.* **10**, 180–182.
- BUSING, W. R. & LEVY, H. A. (1964). *Acta Cryst.* **17**, 142–146.
- CRUICKSHANK, D. W. J. (1961). *J. Chem. Soc.* pp. 5486–5504.
- DAWSON, B., HURLEY, A. C. & MASLEN, V. W. (1967). *Proc. R. Soc. London Ser. A*, **298**, 289–306.
- EYSEL, W., HÖFFER, H. H., KEESTER, K. L. & HAHN, TH. (1985). *Acta Cryst.* **B41**, 5–11.
- ISHIZAWA, N. & KATO, M. (1983). *J. Mineral. Soc. Jpn*, **16**(Special Issue No. 1), 13–20 (in Japanese).
- KIRFEL, A. & WILL, G. (1980). *Acta Cryst.* **B36**, 2881–2890.
- KIRFEL, A. & WILL, G. (1981). *Acta Cryst.* **B37**, 5298–5302.
- MEHROTRA, B. N. (1973). PhD Thesis. Technische Hochschule, Aachen, Germany.
- MEHROTRA, B. N. (1981). *Z. Kristallogr.* **155**, 159–163.
- NARUSE, H., TANAKA, K., MORIKAWA, H., MARUMO, F. & MEHROTRA, B. N. (1987). *Acta Cryst.* **B43**, 143–146.
- SAITO, Y., KOBAYASHI, K. & MARUYAMA, T. (1982). *Thermochim. Acta*, **53**, 289–297.
- SAKATA, M., HARADA, J., COOPER, M. J. & ROUSE, K. D. (1980). *Acta Cryst.* **A36**, 7–15.
- TANAKA, K., KONISHI, M. & MARUMO, F. (1979). *Acta Cryst.* **B35**, 1303–1308.
- TANAKA, K. & MARUMO, F. (1982). *Acta Cryst.* **B38**, 1422–1427.
- TANAKA, K. & MARUMO, F. (1983). *Acta Cryst.* **A39**, 631–641.
- TOKONAMI, M. (1965). *Acta Cryst.* **19**, 486.
- WILLIS, B. T. M. (1969). *Acta Cryst.* **A25**, 277–300.
- YAMANAKA, T., TAKEUCHI, Y. & TOKONAMI, M. (1984). *Acta Cryst.* **B40**, 96–102.

Acta Cryst. (1991). **B47**, 588–597

Characterization of Voids in Crystalline Materials: Application to Oxide Ceramic Systems

BY NOEL W. THOMAS

School of Materials, The University of Leeds, Leeds LS2 9JT, England

(Received 6 July 1990; accepted 25 February 1991)

Abstract

A computer algorithm has been developed for the characterization of voids in all classes of crystalline materials. From the known atomic coordinates, the centres and radii of all voids can be determined. A given void radius corresponds to the radius of the largest sphere which can be located at its centre, without overlapping of that void sphere with coordinating atoms or ions. The methodology is applied in particular to oxide ceramic systems. Since, in these systems, a useful void is one into which a metal cation may be inserted, it must be coordinated solely by oxygen ions. Three polymorphic oxides are con-

sidered in detail: TiO₂, ZrO₂ and WO₃. Dopant ions are identified that are likely to extend the ranges of temperature and pressure over which the individual polymorphs are stabilized. The contribution of the methodology in establishing relationships between chemical composition and crystal structure is also assessed.

Introduction

In most structural studies of crystalline materials, whether metallic, ceramic, polymeric or molecular in nature, attention is focused on the positions and sizes of atoms and ions, with little, or no attention being